Molecular Dynamics Simulation of Liquid Sulfur Dioxide

Mauro C. C. Ribeiro*

Laboratório de Espectroscopia Molecular, Instituto de Química, Universidade de São Paulo, C.P. 26077, CEP 05513−970, São Paulo, SP, Brazil

Received: January 24, 2006; In Final Form: March 16, 2006

A previously proposed model (Sokolić, F.; Guissani, Y.; Guillot, B. *Mol. Phys.* **1985**, *56*, 239) for molecular dynamics (MD) simulation of liquid sulfur dioxide, SO_2, has been reviewed. Thermodynamic, structural, and dynamical properties were calculated for a large range of thermodynamic states. Predicted (P,V,T) of simulated system agrees with an elaborated equation of state recently proposed for liquid SO_2. Calculated heat capacity, expansion coefficient, and isothermal compressibility are also in good agreement with experimental data. Calculated equilibrium structure agrees with X-ray and neutron scattering measurements on liquid SO_2. The model also predicts the same $(SO_2)_2$ dimer structure as previously determined by ab initio calculations. Detailed analysis of equilibrium structure of liquid SO_2 is provided, indicating that, despite the rather large dipole moment of the SO_2 molecule, the structure is mainly determined by the Lennard-Jones interactions. Both single-particle and collective dynamics are investigated. Temperature dependency of dynamical properties is given. The MD results are compared with previous findings obtained from the analysis of inelastic neutron scattering spectra of liquid SO_2, including wave-vector dependent structural relaxation, $\tau(k)$, and viscosity, $\eta(k)$.

Introduction

Sulfur dioxide, SO_2, is fundamental for chemical industry, for instance, in producing sulfuric acid. Designing of industrial plants evidently needs the knowledge of basic physical chemistry properties, and thermodynamic data for SO_2 are extensively tabulated.[1] Melting and boiling points of SO_2 are, respectively, 200.3 and 263.0 K at 1 atm, and its critical point is ($P_c = 78$ atm, $T_c = 157$ K, $V_c = 122$ cm^3 mol^{-1}).[1−3] In condensed phase, SO_2 is an excellent solvent for both organic and inorganic species.[4,5] An elaborated multiparameter equation of state, EoS, has been recently reported for liquid SO_2, including the range of supercritical densities.[6] In the perspective of SO_2 as a solvent, a physical picture of its structure and dynamics on a microscopic basis is also demanding. In fact, liquid SO_2 has been the subject of several spectroscopic investigations, such as NMR,[7] optical Kerr,[8] Raman,[9,10] Brillouin,[11,12] and neutron scattering spectroscopy.[12−16] Molecular dynamics (MD) simulation is an established tool for calculating thermodynamic, structural, and dynamical properties of liquids, but curiously MD investigations of a rather simple liquid as SO_2 are scarce. More than twenty years ago,[17,18] effective pairwise models were proposed for computer simulation of liquid SO_2. The models include Lennard-Jones interactions plus electrostatic interactions represented by either partial charges assigned to sulfur and oxygen atoms or by point dipole and quadrupole interactions. Since then, the first of these models has been used in further MD simulations with specific purposes. For instance, the model has been used for validation of integral equation approximations to the calculation of thermodynamic and structural properties of liquid SO_2.[19] This model has been also used in analyzing neutron scattering spectra of liquid SO_2.[16]

The proposed model for liquid SO_2 has not been the subject of a more systematic validation than one could be able to perform with the computational resources of twenty years ago. In addition, in the last two decades, many other experimental results have become available which one can use to assess the quality of the model. In this work, a thorough MD investigation of liquid SO_2 is performed with the previously proposed model.[17,18] Whereas only four different thermodynamic states were simulated in refs 17 and 18, in this work more than fifty different thermodynamic states were simulated, covering a large range of (P,V,T) conditions. System size simulated in this work is almost 10 times larger, and each MD run is more than twenty times longer. Thus, we are now in a better position to assess the quality of the model. It will be shown that calculated thermodynamic, structural, and dynamic properties are in good agreement with experiment. Thermodynamics of the simulated system was directly compared with the state-of-art EoS for liquid SO_2.[6] Equilibrium structure was compared with neutron scattering measurements[13] and also with the prediction of ab initio calculations for the dimer of SO_2.[20] A single SO_2 molecule has a relatively large dipole moment (1.62 D), but a detailed analysis of MD results indicated that Lennard-Jones interactions are much more decisive in determining the equilibrium structure of the liquid than Coulomb interactions between the partial charges. By calculating several single-particle and collective time correlation functions, dynamics of liquid SO_2 was investigated. The temperature dependency of reorientational relaxation agrees with a very recent investigation of liquid SO_2 by optical-Kerr-effect (OKE) spectroscopy.[8] Spectra of collective excitations were obtained, such as the dynamical structure factor, and both longitudinal and transverse spectra of mass current, i.e., spectra of longitudinal and transverse acoustic (LA and TA) modes.[21−23] In particular, from time correlation functions of TA modes, a wave-vector dependent viscosity, $\eta(k)$, was obtained that agrees with the corresponding result derived from the fit of a viscoelastic model to inelastic neutron scattering data of liquid SO_2.[14,15]

* E-mail: mccribei@iq.usp.br

10.1021/jp060518a CCC: $33.50
Published on Web 04/11/2006

Computational Details

The MD simulations were performed with a potential energy function including short-range Lennard-Jones interactions plus long-range Coulombic interactions between partial charges assigned to the atoms of the SO_2 molecule:

$$U(r_{i\alpha j\beta}) = \sum_{i=1}^{N}\sum_{\alpha=1}^{3}\sum_{j=1}^{N}\sum_{\beta=1}^{3}\left\{4\epsilon_{\alpha\beta}\left[\left(\frac{\sigma_{\alpha\beta}}{r_{i\alpha j\beta}}\right)^{12} - \left(\frac{\sigma_{\alpha\beta}}{r_{i\alpha j\beta}}\right)^{6}\right] + \frac{q_\alpha q_\beta}{r_{i\alpha j\beta}}\right\} \quad (1)$$

where $r_{i\alpha j\beta}$ is the distance between atom α of molecule i and atom β of molecule j, and q_α and q_β are the corresponding partial charges. In refs 17 and 18, four different thermodynamic states were simulated where distinct sets of parameters were tested, including changing the Lennard-Jones parameters for each state. In this work, the MD simulations were performed with a single set of parameters: $\epsilon_{SS}/k_B = 154.4$ K, $\sigma_{SS} = 3.585$ Å, $\epsilon_{OO}/k_B = 62.3$ K, $\sigma_{OO} = 2.993$ Å (see Table 4 in ref 17), where k_B is the Boltzmann constant. The cross-term parameters $\epsilon_{\alpha\beta}$ and $\sigma_{\alpha\beta}$ are given by usual combining rules: $\epsilon_{\alpha\beta} = (\epsilon_{\alpha\alpha}\cdot\epsilon_{\beta\beta})^{1/2}$ and $\sigma_{\alpha\beta} = 1/2(\sigma_{\alpha\alpha} + \sigma_{\beta\beta})$. The partial charges are $q_S = +0.470\ e$, and $q_O = -0.235\ e$. The SO_2 molecule was considered as a rigid body, whose S−O bond length is 1.4321 Å, and the O−S−O angle is 119.5°.

The MD simulations were performed with 1000 SO_2 molecules within a cubic box. Pressure and temperature were controlled with the method of Berendsen et al.[24] of small coupling to an external bath. The equations of motion were solved with the leapfrog algorithm, and a quaternion approach was used for the rotational equations of motion.[25] The time step was 5.0 fs. In each thermodynamic state, the typical equilibration period was 200.0 ps, and the production run was 500.0 ps. MD simulations longer than 1.0 ns were performed to calculate transport coefficients, such as diffusion coefficient and viscosity. The long-range Coulombic interactions were handled with the Ewald sum method.[25]

Results and Discussion

Thermodynamics. The recently proposed equation of state (EoS) for liquid SO_2 is a multiparameter equation for the Helmholtz energy.[6] The advantage of such formulation is that as long as one has an equation for the Helmholtz energy as a function of density and temperature, all of thermodynamic properties can be obtained by appropriate derivatives of this function. In fact, this kind of EoS has been parametrized for many polar and nonpolar fluids.[26] The EoS splits the Helmholtz energy, $\alpha(\tau,\delta)$, into two parts describing the behavior of a hypothetical ideal gas, $\alpha^\circ(\tau,\delta)$, plus a residual part, $\alpha^r(\tau,\delta)$, of the real fluid, where τ is the inverse reduced temperature, $\tau = T_c/T$, and δ is the reduced density, $\delta = \rho/\rho_c$. The elaborated functional forms for $\alpha^\circ(\tau,\delta)$ and $\alpha^r(\tau,\delta)$, and optimized parameters for SO_2, are provided in ref 6. The EoS for SO_2 is valid from 197.7 to 523 K, and pressures up to 35 MPa.[6] Uncertainty in densities ranges from 0.1 to 0.5% from low to high temperatures, and uncertainty in heat capacity is 2.0%.[6] As an example of the EoS, pressure is calculated by derivative with respect to volume:[6,26]

$$\frac{P}{\rho RT} = 1 + \delta\alpha_\delta{}^r \quad (2)$$

where R is the ideal gas constant, and

$$\delta^r{}_\delta = \left(\frac{\partial a^r}{\partial\delta}\right)_\tau$$

Isochoric and isobaric heat capacity, C_V and C_P, need second derivatives:[6,26]

$$\frac{C_V}{R} = -\tau^2 + (\alpha^o_{\tau\tau} + \alpha^r_{\tau\tau}) \quad (3)$$

$$\frac{C_P}{R} = C_V + \frac{(1 + \delta\alpha^r_\delta - \delta\tau\alpha^r_{\delta\tau})}{(1 + 2\,\delta\alpha^r_\delta + \delta^2\alpha^r_{\delta\delta})} \quad (4)$$

where

$$\alpha^o_{\tau\tau} = \left(\frac{\partial^2\alpha^o}{\partial\tau^2}\right)_\delta \quad \alpha^r_{\tau\tau} = \left(\frac{\partial^2\alpha^r}{\partial\tau^2}\right)_\delta \quad \alpha^r_{\delta\delta} = \left(\frac{\partial^2\alpha^r}{\partial\delta^2}\right)_\tau$$

and

$$\alpha^r_{\delta\tau} = \left(\frac{\partial^2\alpha^r}{\partial\delta\partial\tau}\right)$$

In this work, equilibrium (P,V,T) resulting from MD simulations of liquid SO_2 is compared with prediction of the empirical EoS. Figure 1 shows equilibrium molar volume, V_m, as a function of pressure calculated by MD simulations of liquid SO_2 at different temperatures. The MD calculated V_m are lower than experimental values, where the difference between simulation and experiment ranges from 1.7% at 270 K to 2.6% at 210 K. The systematic increase of the error on calculated V_m as temperature decreases is assigned to the potential parameters of the model. In fact, in ref 17 the proposed $\epsilon_{\alpha\alpha}$ were made systematically larger, and $\sigma_{\alpha\alpha}$ smaller, with decreasing temperature. In Figure 1, full lines are isothermals resulting from the empirical EoS,[6] where an average vertical shift of 2.0% has been done in order to illustrate that the slope of simulated isothermals match the experimental ones. Therefore, Figure 1 indicates that the isothermal compressibility, $\kappa_T = -V^{-1}(\partial V/\partial P)_T$, of the simulated system agrees with experimental data. It is worth mentioning that a force field has been recently proposed for MD simulation of SO_2 based on the same functional form as eq 1 for the intermolecular interactions, together with intramolecular contributions of bond stretching and angle bending.[27] By using this flexible model for SO_2 in a single thermodynamic state, the authors of ref 27 obtained 1.3% of difference between simulated and experimental density at 1.0 bar and 223.2 K.

Figure 2 shows the temperature dependency of average potential energy, U, of liquid SO_2 for two isochoric (black symbols) and isobaric (white symbols) conditions. In a given T, it is clear that U is more dependent on V_m than P. The U vs T plot is less steep for isochoric than isobaric condition, as $C_V = (\partial U/\partial T)_V$ is smaller than $C_P = (\partial H/\partial T)_P$, where H is the enthalpy, $H = U + PV$. To calculate heat capacities from the data of Figure 2, one should add the contribution from kinetic energy. This contribution for C_V of SO_2, thought as an ideal gas of (rigid) polyatomic molecules within the harmonic approximation for vibrations, is given by:[28]

$$\frac{C_V}{R} = \frac{3}{2} + \frac{3}{2} + \sum_{i=1}^{3}\left(\frac{\Theta_i}{T}\right)^2 \frac{e^{-\Theta_i/T}}{(1 - e^{-\Theta_i/T})^2} \quad (5)$$

where Θ_i is the vibrational temperature of the normal mode with vibrational frequency ν_i, $\Theta_i = h\nu_i/k_B$, where h is the Planck

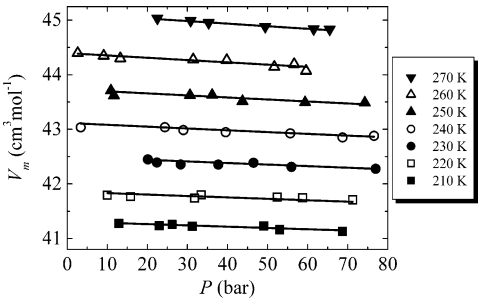

Figure 1. Equilibrium molar volume as a function of pressure calculated by MD simulations of liquid SO_2 at different temperatures (symbols). Full lines are experimental results as predict by the empirical equation of state for liquid SO_2 (eq 2).[6] The full lines were slightly shifted by ca. 2.0% upward in order to illustrate that the isothermal compressibility of the simulated system agrees with experiment.

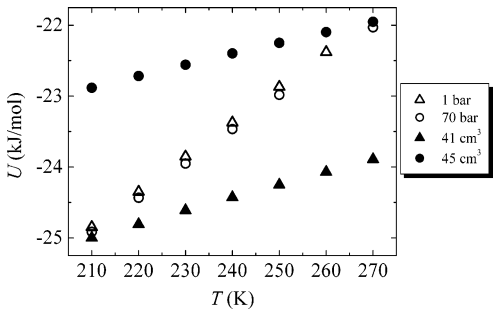

Figure 2. Temperature dependence of average configurational energy calculated by MD simulations of liquid SO_2. Black symbols correspond to isochoric condition; white symbols correspond to isobaric condition.

constant. Wavenumbers of the three normal modes of SO_2 in the gas phase are 1151 cm^{-1} (symmetric stretching mode, ν_1), 518 cm^{-1} (bending mode, ν_2), and 1362 cm^{-1} (antisymmetric stretching mode, ν_3).[29] Thermodynamic functions for SO_2 in the ideal gas state have been calculated by spectroscopic data beyond the rigid-rotator harmonic-oscillator approximation of eq 5.[30] However, if one compares the prediction of eq 5 with this more elaborated calculation (see Table 13 in ref 30), the difference becomes significant only for T higher than ~1000 K. Thus, for the present purpose, the approximation of eq 5 is enough. For the 1 bar isobaric, C_P at 250 K of the simulated system is 87.4 JK^{-1}mol^{-1}, where the configurational contribution responds to 49.3 JK^{-1}mol^{-1}. At this condition, experimental C_P given by eq 4 is 87.2 JK^{-1}mol^{-1}. (It should be noted that simulated and empirical V_m are 43.77 and 42.88 cm^{3}mol^{-1}, respectively, at 1 bar and 250 K.) Thus, there is an excellent agreement between experimental and calculated C_P. The agreement is less satisfactory for C_V. For instance, for the 45.0 cm^3 mol^{-1} isochoric given in Figure 2, C_V at 270 K of simulated system is 45.5 JK^{-1} mol^{-1}, with 15.0 JK^{-1} mol^{-1} being the configurational contribution, whereas experimental C_V given by eq 3 is 52.4 JK^{-1} mol^{-1}. (Simulated SO_2 at 270 K and V_m = 45.0 cm^3 mol^{-1} gives average pressure of 27.8 bar; in such temperature and pressure, empirical V_m is 44.3 cm^3 mol^{-1}). A much worse agreement between calculated and experimental heat capacities, as large as a factor of 2, was claimed in ref 17 and assigned to drawback of the model. However, in ref 17, a rather small system was simulated containing 108 SO_2 molecules by 4000 time steps of simulation, where the heat capacity in a given thermodynamic state was obtained from temperature fluctuations, which might not be a too accurate procedure for evaluating heat capacities.

The slope of V_m vs T curves at constant pressure gives the expansion coefficient, $\alpha_P = V^{-1}(\partial V/\partial T)_P$. It has been found that

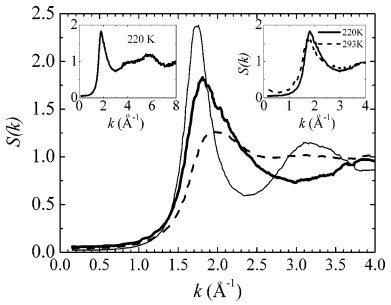

Figure 3. Static structure factor, $S(k)$, of liquid SO_2 simulated at 1 bar and 220 K. The bold line is the total neutron-weighted $S(k)$, thin full line is the partial $S_{SS}(k)$, and dashed line is the partial $S_{OO}(k)$. Left inset display total $S(k)$ in an extended wavevector range. Right inset compares total $S(k)$ at two different temperatures.

α_P of simulated SO_2 also agrees with experimental data.[31] For instance, at 1 bar and 220 K, it was found $(\partial V/\partial T)_P = 0.06$ cm^3 K^{-1} mol^{-1}, whereas experimental value is 0.05 cm^3 K^{-1} mol^{-1} (see Figures 3 and 4 in ref 31).

Structure. The static structure factor, $S(k)$, of liquid SO_2 obtained by X-ray or neutron scattering spectroscopy is dominated by a strong peak at 1.8 Å^{-1}.[13] This is the characteristic feature that should be reproduced by the MD simulations because other peaks observed at k larger than 3.0 Å^{-1} arise from intramolecular correlations, and the model already assumed the known geometry of a single SO_2 molecule. The total $S(k)$ is the combination of partial $S_{\alpha\beta}(k)$ given by:[22]

$$S_{\alpha\beta}(k) = \left\langle \sum_{i=1}^{N} \sum_{\alpha=1}^{3} \sum_{j=1}^{N} \sum_{\beta=1}^{3} e^{i\mathbf{k}(\mathbf{r}_{i\alpha} - \mathbf{r}_{j\beta})} \right\rangle \qquad (6)$$

where α and β stand for either sulfur or oxygen atoms. Each $S_{\alpha\beta}(k)$ is weighted by the molar fraction of the species, x_α and x_β, and by the corresponding neutron scattering length, b_α and b_β, in total $S(k)$ obtained by neutron scattering measurements. The bold line in Figure 3 shows total $S(k)$ calculated by MD simulation of liquid SO_2 at 220 K and 1 bar, using tabulated b_S and b_O, respectively, 2.847 and 5.803 fm.[32] In line with experimental finding,[13] the intermolecular peak at 1.8 Å^{-1} is observed in calculated $S(k)$. The left inset in Figure 3 displays $S(k)$ in an extended k range where intramolecular correlations appear. The peak at 1.8 Å^{-1} is rather broad, and the full thin line and the dashed line in Figure 4 illustrate, respectively, partial $S_{SS}(k)$ and $S_{OO}(k)$ contributions to total $S(k)$. Partial $S_{SS}(k)$ peaks at slightly smaller k; i.e., larger distance in real space, than $S_{OO}(k)$. The right inset shows that a rather large increase in temperature has only a mild effect on calculated $S(k)$. By increasing temperature, $S(k)$ broadens and the main peak shifts slightly to smaller k due to increasing V_m.

Experimental $S(k)$ is usually analyzed by performing a Fourier transform on the crude data in order to obtain the radial distribution function, $g(r)$.[22] Evidently, experimental $g(r)$ is also a weighted combination of partial $g_{\alpha\beta}(r)$. In MD simulations, $g_{\alpha\beta}(r)$ is directly calculated with the known atomic coordinates:[22,25]

$$g_{\alpha\beta}(r) = \frac{V}{N^2} \left\langle \sum_{i=1}^{N} \sum_{\alpha=1}^{3} \sum_{j=1}^{N} \sum_{\beta=1}^{3} \delta(\mathbf{r} - \mathbf{r}_{i\alpha j\beta}) \right\rangle \qquad (7)$$

Figure 4 shows $g(r)$ between center-of-mass calculated by MD simulation of liquid SO_2 at 1 bar and 220 K. The nearest-neighbor shell is characterized by a first peak with maximum at 4.5 Å and minimum at 6.0 Å. The upper inset in Figure 4

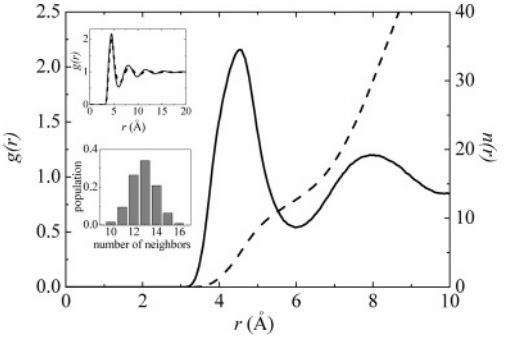

Figure 4. Radial distribution function, $g(r)$, between center-of-mass of liquid SO_2 simulated at 1 bar and 220 K (full line). Dashed line is the running number (eq 8) whose scale is given on the right. Upper inset compares calculated $g(r)$ at 220 K (solid line) and 293 K (dashed line). Lower inset shows histogram of the distribution of nearest neighbor molecules. Molecules were considered nearest neighbors from a given SO_2 molecule as long as their center-of-mass distance is smaller than 6.0 Å, i.e., the position of the first minimum of $g(r)$.

shows the mild temperature effect on $g(r)$, as already noted in $S(k)$ of Figure 3. Upon integration of $g(r)$, one obtains the so-called running number, $n(r)$, which counts the number of molecules in an spherical shell of radius r around a given central molecule:

$$n(r) = \int_0^r \rho g(r') 4\pi r'^2 \, dr' \qquad (8)$$

where ρ is the density. Dashed line in Figure 4 shows $n(r)$ as a function of r, where one finds that there are on average 5 and 13 molecules up to 4.5 and 6.0 Å, respectively, from any central SO_2 molecule. Calculated $g(r)$ agrees with the analysis of experimental $g(r)$, which was modeled by a hypothetical *bcc* arrangement where a given nearest-neighbor SO_2-SO_2 pair was 4.25 Å apart, and each SO_2 molecule was surrounded by 15 molecules.[13] In fact, there is a distribution of nearest-neighbors molecules around any SO_2 molecule, so that $n(r)$ is giving only the average value of such distribution. Counting the number of neighbors included in a spherical shell of chosen radius, and then reporting the distribution of neighbors, provides a more detailed picture of the first shell around a given SO_2 molecule. Taking the first minimum at 6.0 Å in $g(r)$ as the distance characterizing the nearest-neighbors shell, resulting distribution of the number of molecules around a SO_2 molecule is given as histogram in the lower inset of Figure 4. The number of molecules included within this shell ranges from 10 to 16, suggesting that the local environment around SO_2 molecules in the liquid is rather heterogeneous.

The three partials $g_{\alpha\beta}(r)$ are shown as full lines in Figure 5 for liquid SO_2 at 1 bar and 220 K. In each panel of Figure 5, the Lennard-Jones potential for the corresponding pair, $U_{\alpha\beta}(r)$, was superimposed as dotted lines. The position of first maximum of a given $g_{\alpha\beta}(r)$ nicely coincides with the minimum of the corresponding $U_{\alpha\beta}(r)$, suggesting that the equilibrium structure of liquid SO_2 is being determined mainly by the Lennard-Jones interactions. This will be corroborated with further evidences given below. Positions of first peaks in these partials $g_{\alpha\beta}(r)$ agree with the analysis of experimental data provided in ref 13. Small bumps within the spatial range of the first peak in partial $g_{SO}(r)$ and $g_{OO}(r)$ indicate that a pair of SO_2 molecules acquires different relative orientations. However, the analysis of experimental $g(r)$ suggested that several relative orientations could be occurring in liquid SO_2.[13] A similar conclusion was drawn from previous MD simulation.[17] In fact, strong orientational

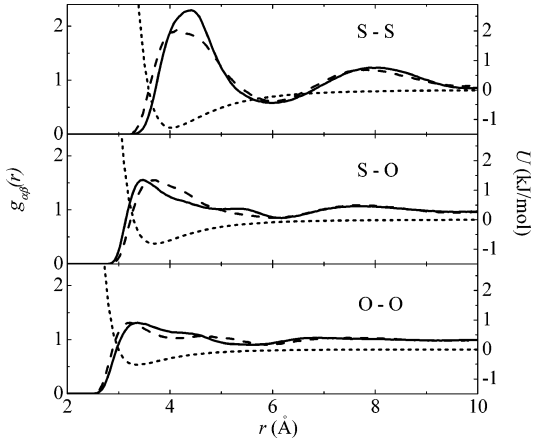

Figure 5. Partial radial distribution functions $g_{SS}(r)$, $g_{SO}(r)$, and $g_{OO}(r)$ (full lines from top to bottom) of liquid SO_2 simulated at 1 bar and 220 K. Dashed lines give $g_{\alpha\beta}(r)$ obtained by a MD simulation run in which no Coulombic interactions were considered by setting all of the partial charges to zero. In each panel, dotted lines show the Lennard-Jones potential function of the corresponding pair with scale on the right.

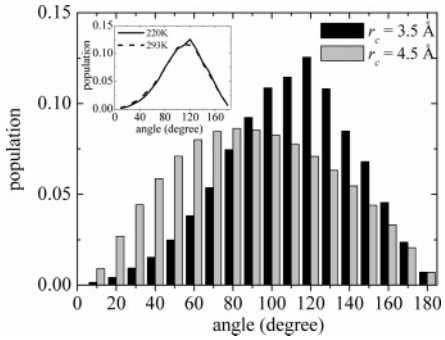

Figure 6. Histograms of the distribution of the angle made by the main symmetry C_2 axis of two neighboring SO_2 molecules. Molecules were considered nearest neighbors from a given SO_2 molecule as long as their center-of-mass distance is smaller than a chosen cutoff radius r_c. Two histograms are shown, corresponding to r_c equal to 4.5 or 3.5 Å. Inset shows the histogram for r_c = 3.5 Å at two different temperatures.

correlations in a pair of SO_2 molecules take place only for a very close approach between the molecules. This is illustrated in Figure 6, which shows the distribution of the angle made by the main symmetry C_2 axis of two neighboring SO_2 molecules, provided that the distance between the molecules is not larger than a chosen radius r_c. The two histograms shown in Figure 6 correspond to chosen r_c of either 4.5 or 3.5 Å. In case of molecules that are 4.5 Å apart, which is the first maximum of $g(r)$ in Figure 4, one already obtains a sinusoidal pattern of angular distribution, proper to randomly orientated directions of dipole moment vectors. Peaked angular distribution at 120° is found only for those molecules that are very close to each other, i.e. $\sim$ 3.5 Å, which is just the distance of a discernible shoulder observed in $g(r)$ in Figure 4. (This pattern of angular distribution is not too temperature dependent, as illustrated in the inset of Figure 6.) This finding agrees with conclusion drawn from the molecular structure factor derived from analysis of inelastic neutron scattering spectra of liquid SO_2.[16] Molecular structure factor follows an uncorrelated approximation up to $k_c \sim 1.5$ Å^{-1}, and then it follows a correlated approximation for higher k. Thus, orientational correlation is expected only for small distances (high-k), and from $r_c \approx 2\pi/k_c$, an orientational correlation length of ca. 4.2 Å was estimated from neutron scattering measurements.[16]

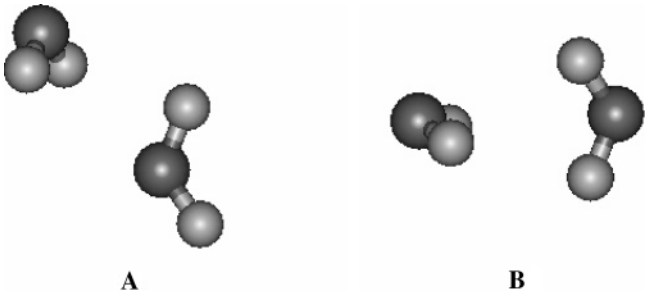

Figure 7. Optimized structure of the $(SO_2)_2$ dimer. Figure A shows the dimmer optimized with the full model (eq 1), which coincides with the ab initio prediction.[20] Figure B is the structure optimized with all of the partial charges set to zero, giving four identical oxygen−oxygen distances and thus optimal Lennard-Jones interactions.

The SO_2 molecule has been the subject of several ab initio quantum chemical calculations mainly devoted to the electronic structure of a single isolated molecule.[33−36] A detailed ab initio investigation of the structure of the $(SO_2)_2$ dimer has been reported, including the effect of considering electronic correlation within the second-order Møller−Plesset perturbation theory.[20] Several stationary points on the dimer potential energy surface were revealed, but a global minimum of C_s symmetry was identified. It has been argued that dispersion forces are the determining factor for the resulting $(SO_2)_2$ structure.[20] Figure 7A shows the $(SO_2)_2$ dimer structure obtained with the present model, which is the same structure derived by ab initio calculation (see Figure 2 of ref 20). Besides confirming that the model is consistent with ab initio calculations, Figure 7 also provides further insight on how the structure is determined by the terms of the potential model of eq 1. In Figure 7A, the planes of the two SO_2 molecules make a 90° angle and two distinct O−O distances occur, the shorter one being 3.45 Å and the larger one being 4.90 Å. This explains the doubled peak pattern observed in the partials $g_{SO}(r)$ and $g_{OO}(r)$ shown in Figure 5. When one optimizes the dimer with the same Lennard-Jones terms, but setting all of the partial charges to zero, i.e., defining a pseudo SO_2 molecule with no dipole moment, the $(SO_2)_2$ dimer acquires the structure shown in Figure 7.B. Without dipole moment and starting from the structure of Figure 7.A, one of the SO_2 molecules rotates giving four identical O−O distances, 3.30 Å, to achieve full optimization of Lennard-Jones interactions. Conversely, when Coulombic interactions are switched on from the optimized structure of Figure 7B, the latter undergoes a slight change on relative orientation that loses optimized Lennard-Jones interactions but favors dipole alignment. Resulting $(SO_2)_2$ dimer structure is the subtle balance of these two contributions.

In condensed phase, the nearest-neighbor shell around a given SO_2 molecule is rather large containing up to 16 molecules (see Figure 4). Thus, in the liquid, it is clear that many relative orientations are allowed, dipole moment alignment being significantly active only for very close approach between two SO_2 molecules (Figure 6). In other words, the above evidences point that equilibrium structure of liquid SO_2 is much more dependent on Lennard-Jones than electrostatic interactions. In fact, by running a MD simulation of liquid SO_2 at 1 bar and 220 K with the same protocol of simulation, but switching off all of the Coulombic interactions, the resulting partial $g_{\alpha\beta}(r)$ of this pseudo liquid SO_2 are not too dissimilar from the correct SO_2 model. Such a comparison is provided in Figure 5. Calculated $g_{\alpha\beta}(r)$ without partial charges (dashed lines) follows closely the correct $g_{\alpha\beta}(r)$ (full lines), with only slight shift on peak positions, and broadening of the first peak of $g_{SS}(r)$.

One gains further insight on the relationship between potential model and resulting equilibrium structure in liquid SO_2 by comparing with other well-investigated polar fluids. For instance, let us consider H_2O and acetonitrile, CH_3CN, two systems that have been the subject of many computer simulations with potential models like eq 1. The well-known extended simple point charge (SPC/E) model for water[37] and a three-site model for CH_3CN[38] gives average values of potential energy at room conditions of −41 and −28 kJ mol^{-1}, respectively. In case of liquid SO_2, average potential energy is −24 kJ mol^{-1} at 1 bar and 220 K. If one decomposes these values into Lennard-Jones and Coulombic contributions, one finds that, for liquid water, the former contributes with +8 kJ mol^{-1} and the latter −49 kJ mol^{-1}. Thus, Coulombic interactions are too stringent in liquid water that H_2O molecules are even allowed to experience the repulsive part of the short-range Lennard-Jones interactions. (In fact, the O···H hydrogen bond distance in liquid water is only 1.8 Å.) In case of CH_3CN, potential energy is more evenly distributed into Lennard-Jones and Coulombic contributions, the former responding for ca. 2/3 and the latter 1/3 of the total potential energy. This is enough for equilibrium structure of liquid CH_3CN displaying clear dipole alignment that is lost when a pseudo (no charge) CH_3CN molecule is simulated (see the bidimensional angular dependent radial distribution functions, $g_{\alpha\beta}(\theta,r)$, shown in Figures 3 and 4 of ref 38). Finally, in case of liquid SO_2, only 1/6 of the total potential energy comes from Coulombic interactions. Therefore, in the sequence of H_2O, CH_3CN, and SO_2, there is a decreasing relative role of dipole interactions on the total potential energy, and, consequently, on the resulting equilibrium structure of the condensed phase.

It should be stressed, however, that the present MD simulations clearly indicate that significant orientational correlation between a pair of SO_2 molecules occurs in the liquid, provided that the two molecules are close together (see Figure 6). This result gives an insight on how short-range can be the orientational effects responsible for the so-called noncoincidence effect observed in Raman spectra of many fluids,[39−41] including liquid SO_2.[9,10] The noncoincidence effect in Raman spectra of liquids is the experimental finding that the wavenumber of a given Raman band in polarized spectra does not match the wavenumber of the same normal mode in depolarized spectra. The mismatch between polarized and depolarized wavenumber reaches 5 cm^{-1} in case of the symmetric stretching mode ν_1 of liquid SO_2.[9,10] The physical origin of the noncoincidence effect is transition dipole coupling between neighboring molecules in an anisotropic local environment due to orientational correlations. Therefore, despite of equilibrium structure of liquid SO_2 being not too dependent on dipole alignment as argued above, the very short-range orientational correlation revealed by MD simulations is still experimentally manifest as the noncoincidence effect in Raman spectroscopy.

Dynamics. Vibrational density of states (DoS) of liquid SO_2 has been estimated from the low wave vector limit of the dynamic structure factor, $S(k,\omega)$, obtained by inelastic neutron scattering spectroscopy.[12] Estimating DoS actually relies on the incoherent part of $S(k,\omega)$, as it has been done for simple liquids containing species with dominant incoherent neutron scattering cross sections.[42] Nevertheless, the relationship between DoS and $S(k,\omega)$ was applied for liquid SO_2:[12]

$$\mathrm{DoS}(\omega) = \frac{2m}{k_B T} \lim_{k\to 0}\left\{\left(\frac{\omega}{k}\right)^2 S(k,\omega)\right\} \qquad (9)$$

where m is the mass. Very recently, similar DoS has been

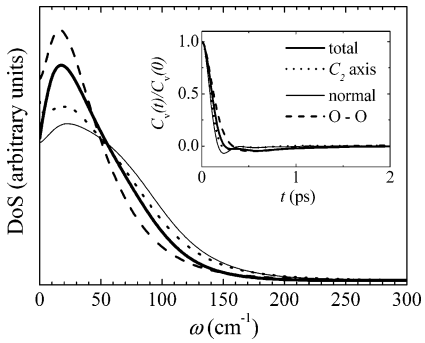

Figure 8. Vibrational density of states (DoS) of liquid SO_2 simulated at 1 bar and 230 K. The total DoS is given by a bold full line. Three projected DoS were obtained by projecting the velocity vector of a given SO_2 molecules into three perpendicular directions: on the C_2 symmetry axis (dotted line), normal to the SO_2 molecular plane (thin full line), and along the line joining the oxygen atoms (dashed line). Inset shows the corresponding velocity correlation functions, from which the DoS were obtained by a Fourier transform.

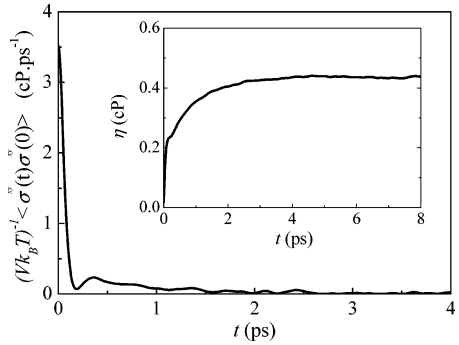

Figure 9. Time correlation function of off-diagonal elements of the stress tensor (eq 11) of liquid SO_2 simulated at 1 bar and 250 K. Inset illustrates the convergence of the time integral of the correlation function, from which viscosity η is obtained.

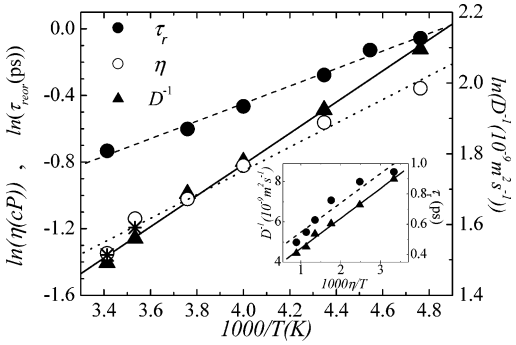

Figure 10. Temperature dependency of reorientational relaxation time of a unitary vector along the C_2 symmetry axis of a given SO_2 molecule, τ_r, viscosity, η, and the inverse of the self-diffusion coefficient, D^{-1}. Inset shows D^{-1} and τ_r as a function of η/T. Lines are fits drawn to MD results.

estimated from OKE spectra, where the DoS is interpreted as librational-orientational short-time dynamics.[8] It should be noted that both neutron scattering and OKE spectra rigorously probe collective dynamics, instead of purely single-particle dynamics. In MD simulations, DoS is directly obtained by Fourier transforming the (single-particle) velocity time correlation function, $C_v(t) = \langle \mathbf{v}_i(t) \cdot \mathbf{v}_i(0) \rangle$. Figure 8 shows as a bold full line the calculated DoS of liquid SO_2 simulated at 1 bar and 230 K. In line with experimental data (see Figure 3 in ref 12, and Figure 6 in ref 8), simulated DoS displays a high-frequency tail. To assign the nature of the DoS shape, the velocity vector $\mathbf{v}_i(t)$ of a given molecule was projected into three perpendicular directions, resulting in projected DoS. It is found that short time rattling dynamics of SO_2 is rather anisotropic. In fact, the inset in Figure 8 shows higher frequency oscillatory pattern of projected $C_v(t)$ on the direction perpendicular to the SO_2 plane than other directions. Consequently, projected DoS cover distinct wavenumber ranges, giving an overall asymmetric shape in total DoS. In the MD simulations of ref 18, reorientational time correlation functions, $C_r(t) = \langle \mathbf{u}_i(t) \cdot \mathbf{u}_i(0) \rangle$, were calculated for unitary vectors $\mathbf{u}_i(t)$ lying along each of the three directions. Distinct decay of $C_r(t)$ for each direction follows the ratio of the moments of inertia of the SO_2 molecule. (The same behavior given in Figure 1 of ref 18 was also obtained here, so that $C_r(t)$ are not shown). Thus, MD simulations reveal anisotropy in both the translational and reorientational single-particle dynamics of liquid SO_2.

It is interesting to compare the temperature dependency of distinct dynamic events in the simulated system. Reorientational relaxation time, τ_r, is obtained by integrating $C_r(t)$. Time integral of $C_v(t)$ gives the self-diffusion coefficient, D, but it was calculated here instead by the linear regime at long time of the mean square displacement:[22]

$$D = \lim_{t \to \infty} \frac{1}{6t} \langle |\mathbf{r}_i(t) - \mathbf{r}_i(0)|^2 \rangle \qquad (10)$$

In addition, shear viscosity, η, was obtained by the time integral of the correlation function of off-diagonal elements of the stress tensor:[22]

$$\eta = \frac{1}{k_B T V} \int_0^\infty \langle \sigma^{xy}(t) \sigma^{xy}(0) \rangle \, \mathrm{d}t \qquad (11)$$

To achieve statistically satisfactory results, η was obtained from typically 1.0 ns long MD runs. The good convergence when calculating η by eq 11 is illustrated in Figure 9 for SO_2 at 1 bar and 250 K.

Figure 10 shows Arrhenius plots of τ_r, η, and D^{-1}. Asterisk symbols in Figure 10 are experimental η of liquid SO_2 at 283 and 293 K reported in Table 1 of ref 11, indicating good agreement between calculated and experimental viscosity. The lines drawn in Figure 10 are linear fits, which highlight the Arrhenius dependence of these dynamical processes. Slopes of linear fits to these plots give similar activation energy, E_a, for these distinct dynamic processes, 5.0 kJ mol^{-1}, although the D^{-1} curve in Figure 10 is slightly steeper than τ_r and η data. Experimentally, $E_a = 4.5$ kJ mol^{-1} has been obtained for τ_r by OKE spectroscopy.[8] In the inset of Figure 10, one sees that the Stokes' law, $D\eta \propto T$, is well obeyed, but a systematic departure from the Stokes−Einstein−Debye relation, $\tau_r \propto \eta/T$, is discernible. In fact, a very similar bended τ_r vs η/T plot was recently obtained from the analysis of OKE spectra of liquid SO_2.[8] The most important conclusion drawn from similar E_a in Figure 10 is the rather strong coupling between translation and reorientation single-particle dynamics probed by τ_r and D, and the dynamics of structural relaxation probed by η.

Further insights on the relationship between structure and dynamics in liquids are given by simultaneous space and time correlation functions. The time dependent generalization of $g(r)$ (see eq 7) is the van Hove correlation function, $G(\mathbf{r},t)$:[22]

$$G(\mathbf{r},t) = \frac{1}{N} \left\langle \sum_{i=1}^{N} \sum_{j=1}^{N} \delta[\mathbf{r} + \mathbf{r}_j(0) - \mathbf{r}_i(t)] \right\rangle \qquad (12)$$

One splits $G(\mathbf{r},t)$ into the self, $G_s(\mathbf{r},t)$, and the distinct, $G_d(\mathbf{r},t)$,

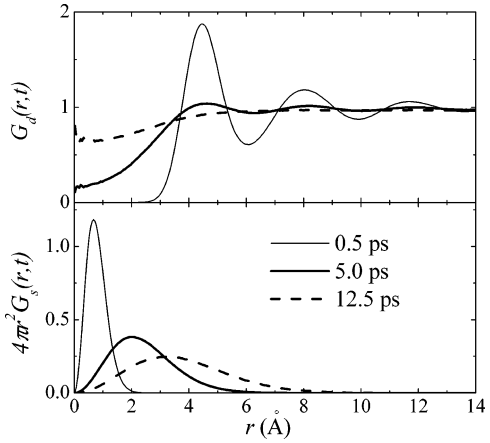

Figure 11. Van Hove correlation function (eq 12) at three different times for liquid SO_2 simulated at 1 bar and 230 K. The top panel shows the distinct term, $G_d(\mathbf{r},t)$, whereas the bottom panel shows the self-term, $G_s(\mathbf{r},t)$.

parts provided that $i = j$ or $i \neq j$, respectively, in eq 12. The $G_s(\mathbf{r},t)$ function provides information on the average displacement of a given molecule at time t, whereas the $G_d(\mathbf{r},t)$ function reveal the time scale in which structural correlation seen in $g(r)$ is lost. Figure 11 shows both $G_s(\mathbf{r},t)$ and $G_d(\mathbf{r},t)$ at three different times for liquid SO_2 simulated at 1 bar and 230 K. From the top panel in Figure 11, one sees that local structure is washed out in a 10.0 ps time scale. On the other hand, in such a time scale, the bottom panel in Figure 11 indicates that the distance travelled by a given SO_2 molecule barely reaches 4.0 Å on average, i.e., the range of the first peak in $g(r)$. Thus, the comparison between $G_s(\mathbf{r},t)$ and $G_d(\mathbf{r},t)$ provided by Figure 11 indicates that structural correlation is being lost in ca. 10.0 ps, but that does not necessarily imply significant translational diffusion in this time range. Consistently, the linear regime of mean square displacement, from which D as reported in Figure 10 were obtained, starts at relatively long time, $t \sim 20.0$ ps.

A space Fourier transform of $G(\mathbf{r},t)$ gives the intermediate scattering function, $F(\mathbf{k},t)$, which provides the time scale of density fluctuations of a given spatial range as selected by the wavevector modulus k.[22] In MD simulations, $F(\mathbf{k},t)$ can be calculated directly by its definition, thus avoiding any numerical artifact of Fourier transformation of the van Hove correlation function:[22]

$$F(\mathbf{k},t) = \left\langle \sum_{i=1}^{N} \sum_{j=1}^{N} e^{i\mathbf{k}\cdot(\mathbf{r}_i(t)-\mathbf{r}_j(0))} \right\rangle \qquad (13)$$

Evidently, $F(\mathbf{k},t)$ can be also split into self-collective parts. To improve statistics of calculated time correlation functions, the average of different $\mathbf{k}$ vectors with the same modulus k is performed, $\mathbf{k} = 2\pi L^{-1}[k_x,k_y,k_z]$. The smallest wavevector available in the simulation is dictated by the size of the cubic box, $k = 2\pi/L[1,0,0]$, which in the present case is ca. 0.15 Å^{-1} depending on the molar volume. The relevant k range is dictated by the static structure factor (see $S(k)$ in Figure 3).

Figure 12 shows both the self-term ($F_s(\mathbf{k},t)$, upper curves) and the collective term (lower oscillatory curves) at three different wavevectors for liquid SO_2 at 1 bar and 210 K. It is clear the slow decay of $F_s(\mathbf{k},t)$, which is consistent with the $G(\mathbf{r},t)$ functions of Figure 11 as the decay rate of $F_s(\mathbf{k},t)$, is dictated by self-diffusion. The collective part displays well-defined oscillations, so that its Fourier transform, i.e., the dynamic structure factor, $S(k,\omega)$, exhibits a resolved peak at nonzero frequency. The oscillation frequency increases with k,

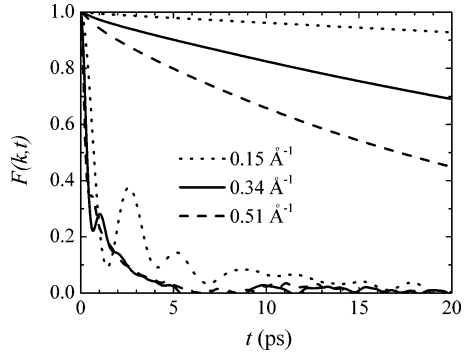

Figure 12. Intermediate scattering function, $F(\mathbf{k},t)$, at three wavevectors for liquid SO_2 simulated at 1 bar and 210 K. The three upper slowing decaying curves are self-terms, whereas the three lower oscillatory curves are distinct terms.

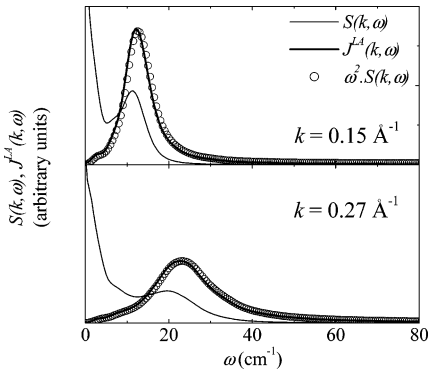

Figure 13. Thin line: dynamic structure factor, $S(k,\omega)$. Bold full line: spectra of LA modes, $J^{LA}(k,\omega)$. White circles: the product $\omega^2 \cdot S(k,\omega)$, for liquid SO_2 simulated at 1 bar and 210 K. The upper panel correspond to $k = 0.15$ Å^{-1}, and the bottom panel to $k = 0.27$ Å^{-1}.

so that there is dispersion of excitation energy, $\omega(k)$. This is seen easier in $S(k,\omega)$, as illustrated in Figure 13 for two different wavevectors. In MD simulations of liquids, collective excitations have been investigated either in $S(k,\omega)$ or in spectra of time correlation functions of longitudinal mass current fluctuations, $C(k,t) = \langle j(k,t) \cdot j^*(k,0) \rangle$.[21−23,43−47] The appropriate mass current for longitudinal acoustic (LA) modes is

$$j^{LA}(k,t) = \sum_{i=1}^{N} m_i \hat{\mathbf{k}} \cdot \mathbf{v}_i(t) e^{-ik\mathbf{r}_i(t)} \qquad (14)$$

where m_i is the mass, $\mathbf{v}_i$ is the velocity, and $\mathbf{r}_i$ is the coordinate of the center of mass of molecule i. The advantage of calculating LA spectra, $J^{LA}(k,\omega)$, is that a peak is observed in $J^{LA}(k,\omega)$, even when the oscillation is too damped for any discernible peak being observed in $S(k,\omega)$. However, the same information on collective excitations is contained in both $J^{LA}(k,\omega)$ and $S(k,\omega)$, because they are directly related to each other, $J^{LA}(k,\omega) = (\omega^2/k^2)S(k,\omega)$. As a consistency check, Figure 13 shows that $J^{LA}(k,\omega)$ (bold full line) in fact coincides with $\omega^2 S(k,\omega)$ (white circles) in case of liquid SO_2.

Propagating collective excitations in liquid SO_2 has been already the subject of a detailed investigation by neutron scattering spectroscopy.[12,14−16] Experimental neutron scattering spectra were quantitatively reproduced by MD simulations with the same model as used in this work (eq 1).[16] One of the main conclusions drawn from the comparison between experimental and simulated spectra[16] was orientational correlation between SO_2 molecules in close approach (see the discussion of Figure 6 above). On analyzing neutron spectra,[14,15] experimental data

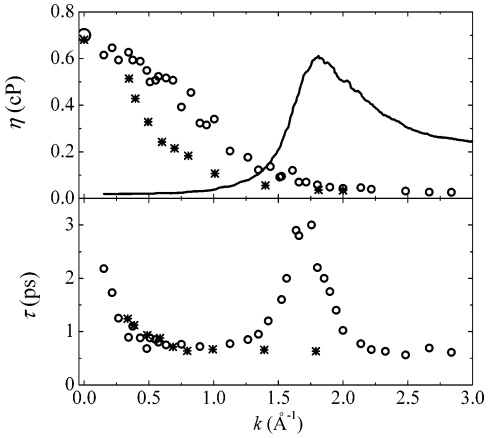

Figure 14. Upper panel: wavevector dependent viscosity $\eta(k)$ (eq 15) of liquid SO_2 simulated at 1 bar and 210 K (white circles) and corresponding experimental result of ref 15 (asterisks). The large circle at zero k is the viscosity η calculated directly by the time correlation function of stress tensor (eq 11). Full line is the calculated $S(k)$ in an arbitrary scale. Bottom panel: structural relaxation time, $\tau(k)$, obtained by the time integral of $F(\mathbf{k},t)$ (eq 13) for liquid SO_2 simulated at 1 bar and 210 K (white circles) and corresponding experimental result of ref 15 (asterisks).

were fit to a viscoelastic model, in which the two adjustable parameters are the second and fourth frequency moments of $S(k,\omega)$. These parameters are wavevector dependent, from which relaxation time, $\tau(k)$, and a generalized k-dependent viscosity, $\eta(k)$, were obtained.[14,15]

In this work, the experimentally derived $\tau(k)$ and $\eta(k)$ are compared with direct calculations from MD simulations of liquid SO_2. Structural relaxation time $\tau(k)$ was obtained as the time integral of collective $F(\mathbf{k},t)$ (see Figure 12). Wavevector dependent viscosity can be obtained by time correlation functions of transverse mass current fluctuations analogous to eq 14. Spectra of transverse acoustic (TA) modes, $J^{TA}(k,\omega)$, allow one to estimate $\eta(k)$ by its $\omega \rightarrow 0$ limit:[23,48−50]

$$\eta(k,\omega=0) = \frac{\rho}{k^2}\frac{1}{J^{TA}(k,\omega=0)} \qquad (15)$$

where ρ is the density. In other words, $J^{TA}(k,\omega=0)$ is the time integral of the correlation function of transverse mass current. The $k \rightarrow 0$ limit of $\eta(k)$ gives the macroscopic viscosity η, which must be consistent with the direct calculation from time correlation function of the stress tensor (eq 11). Figure 14 shows $\tau(k)$ and $\eta(k)$ obtained by MD simulation of liquid SO_2 at 1 bar and 210 K (white circles) together with the corresponding experimental results (asterisks) given in Figure 2 of ref 15. To illustrated the relevant wave vector range, the full line in the top panel of Figure 14 shows the calculated $S(k)$. In the top panel of Figure 14, the large white circle at zero k is the viscosity η calculated by eq 11, which coincides with the low-k limit of simulated $\eta(k)$. There is a reasonable agreement between experimental and simulated $\eta(k)$, adding a further validation test of the proposed model for liquid SO_2.[17,18] Simulated $\tau(k)$ increases in the range of the main peak of $S(k)$, i.e., calculated $F(\mathbf{k},t)$ display a remarkable slowing down due to persistent structural correlations when k reaches the peak of $S(k)$. The few best fit parameters $\tau(k)$ provided in ref 15 do not indicate increasing relaxation time at the main peak of $S(k)$. The bottom panel in Figure 14 shows that $\tau(k)$ reaches a rather constant value of ca. 0.65 ps at high k. This time scale of structural relaxation is the same as the reorientational relaxation, for instance, simulated τ_r given in Figure 10 is 0.95 ps at 210 K. (In ref 14, when modeling experimental neutron spectra, it was used $\tau_r = 0.95$ ps as had been previously reported by NMR spectroscopy in ref 51; the same range of τ_r values was also obtained by OKE spectroscopy in ref 8.) Therefore, the MD simulations strongly suggest that significant coupling between reorientational dynamics and structural relaxation occurs in liquid SO_2.

Conclusions

An extensive comparison between simulation results and experimental data has been performed, showing that the proposed model of Sokolić et al.[17,18] is a good one for thermodynamic, equilibrium structure, and dynamics of liquid SO_2. For many thermodynamic states, the difference between calculated and experimental[6] molar volume is ca. 2.0%. The model also predicts heat capacity, expansion coefficient, and isothermal compressibility, in good agreement with experiments. Equilibrium structure of the simulated system is consistent with both experimental[13] and ab initio results.[20] Comparison between neutron scattering and MD results was performed in both the real space and in the reciprocal space. Theoretical calculations of the structure of $(SO_2)_2$ dimer were published after the proposition of the potential model of ref 17, and the latter in fact predicts the same minimum global structure as ab initio calculations. The ab initio investigation on $(SO_2)_2$ dimer suggested that dispersion interactions are the relevant contributions for the overall structure of the dimer.[20] The MD simulations also indicated that Lennard-Jones interactions dominate in liquid SO_2, so that strong orientational correlation dictated by dipole interaction prevail only for pair of molecules in close approach. The model is also a reasonable one as concerning dynamical properties, either single-particle or collective dynamics. Proper to similar decaying rate observed for several time correlation functions of distinct properties, the MD simulations suggest strong coupling between different dynamics process, such as translation, reorientation, structural relaxation, and viscosity. The agreement between experimental[14,15] and simulated wavevector dependent viscosity $\eta(k)$ is a stringent test on the model, as the generalized $\eta(k)$ simultaneously probes space and time correlations.

Acknowledgment. The author is indebted to FAPESP and CNPq for financial support.

References and Notes

(1) Dortmund Data Bank for Pure Component Properties (DDB−Pure), DDBST GmbH, Oldenburg, Germany, 2002 (http://www.ddbst.de).
(2) Kang, T. L.; Hirth, L. J.; Kobe, K. A.; McKetta, J. J. *J. Chem. Eng. Data* **1961**, *6*, 220.
(3) Yaws, C. L.; Li, K. Y.; Kuo, C. H. *Chem. Eng.* **1974**, *81*, 85.
(4) Burow, D. F. In *Chemistry of Nonaqueous Solvents*; Logowski, J., Ed.; Academic Press: New York, 1970.
(5) Eisfeld, W.; Regitz, M. *J. Am. Chem. Soc.* **1996**, *118*, 11918, and references therein.
(6) Ihmels, E. C.; Lemmon, E. W.; Gmehling, J. *Fluid Phase Equilib.* **2003**, *207*, 111.
(7) Makulski, W.; Jackowski, K. *J. Mol. Struct.* **2004**, *704*, 219.
(8) Jaye, A. A.; Hunt, N. T.; Meech, S. R. *J. Chem. Phys.* **2006**, *124*, 024506.
(9) Kamoun, M. *J. Raman Spectroc.* **1979**, *8*, 225.
(10) Brooker, M. H.; Eysel, H. H. *J. Phys. Chem.* **1984**, *88*, 6201.
(11) Musso, M.; Aliotta, F.; Vasi, C.; Aschauer, R.; Asenbaum, A.; Wilhelm, E. *J. Mol. Liq.* **2004**, *110*, 33.
(12) Chahid, A.; García-Hernández, M.; Prieto, C.; Bermejo, F. J.; Enciso, E.; Martínez, J. L. *Mol. Phys.* **1993**, *78*, 821.
(13) Yamaguchi, T.; Lindqvist, O.; Dahlborg, U. *Acta Chem. Scand.* **1984**, *38*, 757.
(14) Martínez, J. L.; Bermejo, F. J.; García-Hernández, M.; Mompeán, F. J.; Enciso, E.; Martín, D. *J. Phys.: Condens. Matter* **1991**, *3*, 4075.

(15) Bermejo, F. J.; Martínez, J. L.; Martín, D.; García-Hernández, M.; Mompeán, F. J.; Alonso, J. *J. Chem. Phys.* **1991**, *95*, 5387.
(16) Dawidowski, J.; Chadid A.; Bermejo, F. J.; Enciso, E.; Almarza, N. G. *Phys. Rev. E* **1995**, *52*, 2787.
(17) Sokolić, F.; Guissani, Y.; Guillot, B. *Mol. Phys.* **1985**, *56*, 239.
(18) Sokolić, F.; Guissani, Y.; Guillot, B. *J. Phys. Chem.* **1985**, *89*, 3023.
(19) Alvarez, M.; Lado, F.; Lomba, E.; Lombardero, M.; Martín, C. *J. Chem. Phys.* **1997**, *107*, 4642.
(20) Bone, R. G. A.; Le Sueur, C. R.; Amos, R. D.; Stone, A. *J. Chem. Phys.* **1992**, *96*, 8390.
(21) Boon, J. P.; Yip, S. *Molecular Hydrodynamics*; Dover: New York, 1980.
(22) Hansen, J. P.; McDonald, I. R. *Theory of Simple Liquids*; Academic Press: London, 1990.
(23) Balucani, U.; Zoppi, M. *Dynamics of the Liquid State*; Oxford University Press: Oxford, 1994.
(24) Berendsen, H. J. C.; Postma, J. P. M.; Gunsteren, W. F.; DiNola, A.; Haak J. R. *J. Chem. Phys.* **1984**, *81*, 3684.
(25) Allen, M. P.; Tildesley, D. J. *Computer Simulation of Liquids*; Oxford University Press: Oxford, 1987.
(26) Span, R.; Wagner, W. *Int. J. Thermophys.* **2003**, *24*, 1.
(27) Yang, J.; Ren, Y.; Tian, A.; Sun, H. *J. Phys. Chem. B* **2000**, *104*, 4951.
(28) McQuarrie, D. A.; Simon, J. D. *Physical Chemistry*; University Science Books: Sausalito, CA, 1997.
(29) Herzberg, G. *Molecular spectra and molecular structure, Infrared and Raman spectra of polyatomic molecules*; Van Nostrand: New York, 1945.
(30) McBride, B. J.; Gordon, S. *J. Chem. Phys.* **1961**, *35*, 2198.
(31) Miskiewicz, S.; Rieser, K.; Dorfmüller, T. *Ber. Bunsen-Ges. Phys. Chem.* **1976**, *80*, 395.
(32) http://www.ncnr.nist.gov/resources/n-lengths/.
(33) Bundgen, P.; Grein, F.; Thakkar, A. *J. Theochem. J. Mol. Struct.* **1995**, *334*, 7.
(34) Martin, J. M. L. *J. Chem. Phys.* **1998**, *108*, 2791.
(35) Xenides, D.; Maroulis, G. *Chem. Phys. Lett.* **2000**, *319*, 618.
(36) Wilson, A. K.; Dunning, T. H., Jr. *J. Chem. Phys.* **2003**, *119*, 11712.
(37) Berendsen, H. J. C.; Grigera, J. R.; Straatsma, T. P. *J. Phys. Chem.* **1987**, *91*, 6269.
(38) Terzis, A. F.; Samulski, E. T. *Chem. Phys. Lett.* **1996**, *251*, 157.
(39) Torii, H.; Musso, M.; Giorgini, M. G.; Doge, G. *Mol. Phys.* **1998**, *94*, 821.
(40) Tukhvatullin, F. H.; Pogorelov, V. E.; Tashkenbaev, U. N.; Jumaboev, A.; Hushvaktov, H.; Seit-Enon, M.; Osmanov, S. A. *J. Raman Spectrosc.* **2003**, *34*, 813.
(41) Uemura, T.; Saito, S.; Mizutani, Y.; Tominaga, K. *Mol. Phys.* **2005**, *103*, 37.
(42) Carneiro, K. *Phys. Rev. A* **1976**, *14*, 517.
(43) Ribeiro, M. C. C.; Wilson, M.; Madden, P. A. *J. Chem. Phys.* **1998**, *108*, 9027.
(44) Sette, F.; Krisch, M. H.; Masciovecchio, C.; Ruocco, G.; Monaco, G. *Science* **1998**, *280*, 1550.
(45) Ruocco G.; Sette, F. *J. Phys.: Condens. Matter* **1999**, *11*, R259.
(46) Ribeiro, M. C. C. *J. Chem. Phys.* **2001**, *114*, 6714.
(47) Pontecorvo, E.; Krisch, M.; Cunsolo, A.; Mônaco, G.; Mermet, A.; Verbeni, R.; Sette, F.; Ruocco, G. *Phys. Rev. E* **2005**, *71*, 011501.
(48) Alley, W. E.; Alder, B. J. *Phys. Rev. A* **1983**, *27*, 3158.
(49) Palmer, B. J. *Phys. Rev. E* **1994**, *49*, 359.
(50) Balucani, U.; Brodholt, J. P.; Jedlovszky, P.; Vallauri, R. *Phys. Rev. E* **2000**, *62*, 2971.
(51) Wasylishen, R. E.; McDonald, J. B.; Friedrich, J. O. *Can. J. Chem.* **1984**, *62*, 1181.